IEEE Access
Multidisciplinary | Rapid Review | Open Access Journal

Received 16 October 2024, accepted 4 November 2024, date of publication 8 November 2024,
date of current version 26 November 2024.

Digital Object Identifier 10.1109/ACCESS.2024.3493934

RESEARCH ARTICLE

Transient Synchronization Stability Modeling and Analysis of Grid-Following Converter Considering Current Dynamics

TEKLU DEREJE, LING ZHAN, BIN HU, (Member, IEEE), AND HENG NIAN, (Senior Member, IEEE)
College of Electrical Engineering, Zhejiang University, Hangzhou 310027, China

Corresponding author: Heng Nian (nianheng@zju.edu.cn)

This work was supported in part by the National Natural Science Foundation of China under Grant 52325702, and in part by China Postdoctoral Science Foundation under Grant 2024T170766.

ABSTRACT The increasing integration of converter-based energy sources, in the modern power grid has brought a significant challenge in the form of transient instability of grid-following converters (GFCs). Existing research on transient stability merely centered on phase looked loop (PLL) dynamics while the current control loop is ignored. However, in the scenario of a high power GFC connected with weak grid, it is not possible to approximate the current loop dynamics as a unit gain, since the low switching frequency of high-power converters does not allow for high current loop bandwidth. This paper finds that slow current dynamics together with the weak grid's characteristics might deteriorate the transient stability of GFC when the system is subjected to a shallow grid voltage drop. Accordingly, a sixth-order nonlinear model is proposed to describe the coupling effect between the current loop and PLL. The accuracy of the model is confirmed through time-domain simulation and parameter sensitivity analysis is performed. Finally, theoretical analysis is validated through experimental tests.

INDEX TERMS Grid-following converter, phase looked loop, current control loop, transient stability.

I. INTRODUCTION

The increasing demand for energy has resulted in a significant rise in the utilization of voltage source converters (VSC) for grid connected renewable energy sources [1], [2], [3]. The majority of VSCs are operated in current control mode, also known as grid-following converters (GFC), which employ the phase-locked loop (PLL) to achieve grid synchronization [4], [5]. The power processing mechanism of GFC presents a stability challenge in contrast to synchronous generators (SGs) [6]. The grid code with the low voltage ride through (LVRT) requirement helps the GFC to have robust ability against fault in some extent [7], [8]. Nevertheless, multiple studies have shown that GFCs still face challenges in maintaining synchronization when confronted with substantial grid faults [9], [10], [11], [12]. Thus, conducting an analysis on transient stability holds immense importance.

In this regard, the second-order nonlinear model is developed to assess the transient stability of the GFC centered on equilibrium points and the damping ratio [13], [14], [15]. In [13], it is stressed that the absence of equilibrium points can ultimately lead to loss of synchronization (LOS). In weak grid scenarios, significant voltage drops increases the vulnerability of PLL to losing its stable equilibrium point (SEP) [14], and can cause a decrease in the damping ratio of the PLL [15], thus might leading to transient instability. In [16], reducing PLL parameters, like settling time and damping ratio, might negatively impact the transient stability of GFC. In [17], [18], [19], and [20] reveals transient instability mechanism through equal area criterion (EAC). The study in [17] found that LOS is mainly caused by the unbalanced input of PLL. However, this issue can be mitigated by appropriate adjustments to the current injection references [18] [19] introduces

The associate editor coordinating the review of this manuscript and approving it for publication was Pinjia Zhang.

a method for normalizing the PLL, while [20] presents an adaptive damping technique aimed at addressing grid faults and improving system stability. Transient stability of the GFC is also influenced by initial state and dynamic characteristics of system [21], it has been pointed out that a large value of initial angle speed can pose a threat to the transient stability.

The literature mentioned earlier predominantly centers on the dynamics of PLL, overlooked the dynamics of the current control loop, as it is assumed to be a unit gain. Less studies analyzed the impact of current control loop on the synchronization dynamics. In [22], presents the effect of current dynamics through large-signal model. However, the analysis is focused on GFCs filter inductance and current controller time constant. The impact of a lower current loop bandwidth on transient stability is investigated through fourth-order model in [23], which considers only the effects of active current dynamics under stiff grid conditions while overlooks reactive current dynamics. Furthermore, [24] proposes a fourth-order model to show relationship between injected reactive current and grid inductance, which has a crucial role in transient stability. However, this study is conducted within a context of very high current loop bandwidth.

To this end, none of the works mentioned above provide a comprehensive analysis of the transient stability of GFC, taking into consideration the coexisting factors of a weak grid and a lower current loop bandwidth. There still lacks a comprehensive understanding regarding the connection between grid strength and current loop bandwidth, and how they collectively impact transient stability. Therefore, in order to understand the underlying issues, this paper built a refined model which helps to analyze the impact of current loop bandwidth under weak grid condition, thus helps to obtain the optimal stable region by tuning current controller parameter while after setting PLL parameter.

Our study on transient stability modeling is significantly based on a single grid-connected converter configuration, highlighting notable advancements in the accuracy and reliability of transient stability predictions. Additionally, this work aids in selecting the appropriate current loop bandwidth in weak grid scenarios. Furthermore, with the knowledge gained from the analysis of single-grid connected converter system, our research lays a foundation for analyzing transient stability phenomena in multi-grid connected converter systems qualitatively. This approach is also crucial for enhancing the reliability and efficiency of interconnected power systems.

The contributions of this paper can be concluded as follows:

1) To analyze the coupling mechanism between the current loop and PLL during the transient process, it has been demonstrated that the traditional second-order synchronization model may result in incorrect stability assessments in situations characterized by low current loop bandwidth.

2) Considering the coupling behavior of the current loop and PLL, a sixth-order model is proposed to replace the second-order model to accommodate all current loop bandwidth applications.

3) Based on our proposed sixth-order model, we reveal the bandwidth boundary where the current loop dynamics can be ignored, which provides design guidance for practical engineering applications.

The rest of this paper is organized as follows. Section II provides a comprehensive overview of the GFC's topology and synchronization dynamics. It also highlights the limitations of the traditional second-order model, leading to the introduction of a sixth-order model in Section III. Section IV validates the accuracy of the proposed model and performs sensitivity analysis of key parameters. Section V presents the experimental findings, and Section VI concludes the work.

II. CONVETIONAL TRANSIENT SYNCHRONIZATION MODEL OF GRID FOLLOWING CONVERTER

In this section, the topology of the system under investigation is presented, and the conventional transient synchronization model of the GFC is established, with a focus on the interaction between the PLL and grid impedance.

A. SYSTEM DESCRIPTION

Figure 1 illustrates the topology and control block diagram of GFC connected to an AC grid. The terminal voltage of the GFC is denoted by u_{gfc}. The magnitude and phase of the voltage at the point of common coupling (PCC) are represented by u_{pcc} and θ_{pcc}, respectively. The magnitude and phase of the voltage at the grid connection point (GCP) are denoted by u_{gcp} and θ_{gcp}. The filter and grid inductors are symbolized by L_f and L_g, respectively. V_{dc} is dc-link voltage.

As shown in Figure 1, the current source functionality of GFC is demonstrated, with its control managed by PLL. The magnitude and phase of current injected into the AC grid by GFC are represented by I_{pcc} and $\theta_{pll} + \phi$, respectively. θ_{pll} is the output from PLL, and ϕ can be obtained through $\tan^{-1}(I_q/I_d)$, where I_d and I_q denote the active and reactive current, respectively, and are determined by the current control loop. I_d^* and I_q^* are used to represent active and reactive current references, respectively.

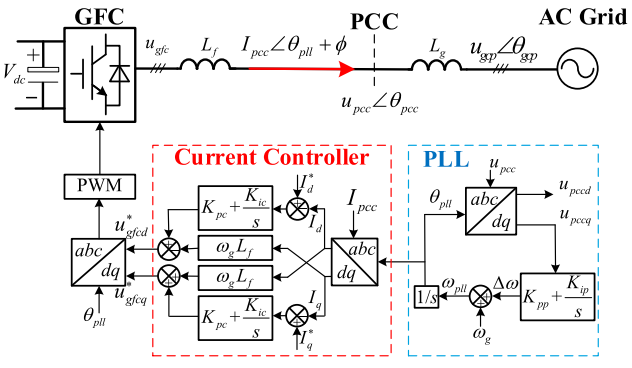

FIGURE 1. Topology of GFC connected with inductive grid.

The current regulation system utilizes proportional gain (K_{pc}) and integral gain (K_{ic}) controllers in the current control loop to achieve accurate and fast current control response.

Moreover, $\omega_g L_f I_d$ and $\omega_g L_f I_q$ serve as decoupling terms, which helps to secure independent control of the two channels.

In Figure 1, the PLL is used to synchronize the GFC with the grid, a task completed likely by adjusting the proportional gain (K_{pp}) and integral gain (K_{ip}). The fundamental angular frequency ω_g is 100π rad/s. The PLL detects the angular frequency as ω_{pll}, and the difference between ω_{pll} and ω_g is represented as $\Delta\omega = \omega_{pll}$-$\omega_g$. In the steady state, when $\omega_g = \omega_{pll}$, $\Delta\omega$ is 0, and θ_{pll} equals to θ_{pcc}.

The control dynamics of the PLL can be expressed as

$$\theta_{pll} = \int \left[\left(K_{pp} + K_{ip}\int\right) u_{pccq} + \omega_g\right] \tag{1}$$

where u_{pccq} symbolizes the q-axis component of u_{pcc}, under pure inductive grid, mathematically can be expressed as

$$u_{pccq} = -u_{gcp}\sin\left(\theta_{pll} - \theta_{gcp}\right) + \omega_{pll} L_g I_d \tag{2}$$

B. CONVENTIONAL SECOND-ORDER SYNCHRONIZATION MODEL

In the GFC scenario, transient stability focuses more on the dynamics of the PLL rather than the current control loop. This is because the inner current loop is typically designed to operate at a higher bandwidth compared to the synchronization control loop [14].

In synchronization dynamics, δ represents the difference between θ_{pll} and θ_{gcp}. By substituting (2) into (1) and equating θ_{gcp} to $\int \omega_g\, dt$, we can calculate the value of δ as follows

$$\delta = \int \left(K_{pp} + K_{ip}\int\right)\left(-u_{gcp}\sin\delta + \omega_{pll} L_g I_d\right) \tag{3}$$

When the u_{gcp} drops from nominal voltage (u_{nom}) to a certain value of a fault voltage (u_{fault}), considered frequency variation as $\Delta\omega = \omega_{pll}$-$\omega_g$, it is important to note that $\Delta\omega$ is also equivalent to δ', the superscript "$'$" denotes differential notation. To express the transient process, upon differentiating both sides of (3) twice, it yields (4) as follows

$$\delta'' = \frac{K_{pp}\left(-u_{fault}\cos\delta\delta'\right)}{1 - K_{pp} L_g I_d^*} + \frac{K_{ip}\left(-u_{fault}\sin\delta + \left(\omega_g + \delta'\right) L_g I_d^*\right)}{1 - K_{pp} L_g I_d^*} \tag{4}$$

The presence of an equilibrium point alone does not determine systems dynamic behavior, transient instability in the GFC can still occur due to the initial values of the system's state, as evidenced by references [21], [23], [24].

$$\delta_i = \sin^{-1}\frac{\omega_{pll} L_g I_d}{u_{gcp}} \tag{5}$$

$$\delta_i' = \frac{K_{pp}\left(-u_{fault}\sin\delta_i + \omega_g L_g I_d^*\right)}{1 - K_{pp} L_g I_d^*} \tag{6}$$

This paper will give some cases that u_{gcp} drops from $u_{nom} = 1$ per unit (p.u.) to u_{fault} of 0.66 p.u., while under different grid strength and current loop bandwidth (f_c), The GFC provides 2% reactive current per percent of the voltage drop according to grid code. The circuit and controller parameters are listed in Table 1, where the slower f_c is 150 Hz, and the faster f_c is 500Hz.

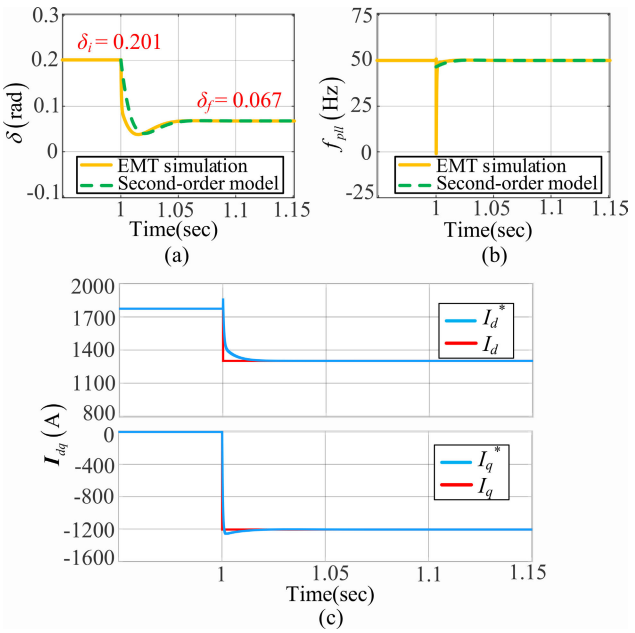

FIGURE 2. Dynamic response when u_{fault} is 0.66 p.u., L_g is 0.2 p.u., R_g is 0.2 p.u. and f_c = 500Hz (a) angle response. (b) frequency response. (c) current response.

The frequency at which a power converter operates, known as the switching frequency (f_{sw}), accordingly is set to 2 kHz in this paper. A higher f_{sw} can result in smaller component sizes and improved transient response, but it may also lead to increased switching losses and electromagnetic interference [25]. Conversely, a lower switching frequency can enhance efficiency by reducing these losses, yet it may require larger components and result in slower response times [26]. Therefore, selecting an appropriate switching frequency in conjunction with the current loop bandwidth is essential for proper functionality and reliability of grid connected power converters. To analyze the transient stability of GFC, where the real-time electromagnetic transients (EMT) based simulation are carried out in MATLAB/Simulink.

Accordingly, Figures 2 and 3 illustrate the impact of faster and slower f_c under strong grids condition, when u_{gcp} drops to u_{fault} of 0.66 p.u. Under such case, as seen from Figures 2(c) and 3(c), the dynamic response of injected current exhibit fast response, i.e both active and reactive current complete transient process and follows the reference quickly.

Figures 2(a) and 3(a) demonstrate the angle responses, while Figures 2(b) and 3(b) depict the frequency responses, showed that, the prediction by the second-order model is similar with Electromagnetic transient (EMT) simulation result. Thus, the second-order model is enough to predict the

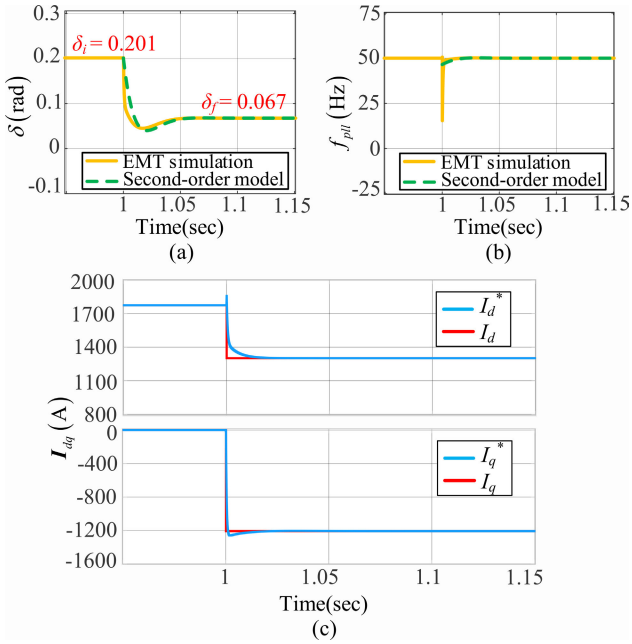

FIGURE 3. Dynamic response when u_{fault} is 0.66 p.u., L_g is 0.2 p.u., R_g is 0.2 p.u. and f_c = 150Hz. (a) angle response, (b) frequency response and (c) current response.

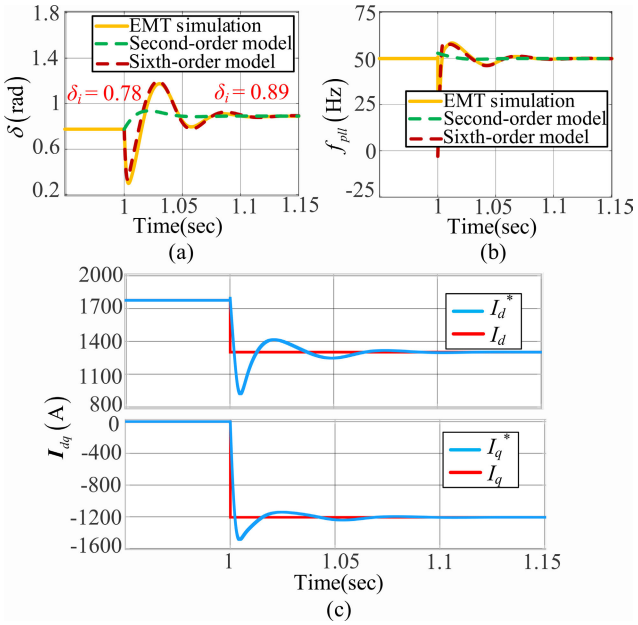

FIGURE 4. Dynamic response when u_{fault} is 0.66 p.u., L_g is 0.7 p.u., R_g is 0 p.u. and f_c = 500 Hz. (a) angle response, (b) frequency response and (c) current response.

transient stability of GFC while under strong grid with faster and slower f_c. In general, in a stiff grid scenario, it can be observed that, the f_c has a negligible impact on the transient stability of GFC, i.e no matter how the f_c is fast or slow, the system is always stable in such scenario.

On the other case, when u_{gcp} drops to u_{fault} of 0.66 p.u., under weak grid strength, the impact of faster and slower f_c is observed by Figure 4 and 5, respectively. As seen from Figure 4(c), the injected active and reactive current exhibit slow dynamics response in the larger f_c. Angle and frequency response of system indicated by Figure 4(a) and Figure 4(b), respectively, the EMT simulation result shows that there is a large angle deviation and frequency fluctuation, this phenomenon cannot be captured by the second-order model, and it may lead to wrong transient stability prediction.

As shown in Figure 5 (c), when f_c is lower, the dynamic response of injected active and reactive current is significantly slower. Also as seen in Figure 5(a) and Figure 5(b), there is significant difference in the stability prediction between EMT simulation output and second-order model, when the EMT simulation indicates LOS, the second-order model predicts that the system remains stable.

In general, weak grid with lower f_c, if the transient stability analysis merely considered impact of PLL, the results will definitely deviate, or even presents wrong conclusion. Therefore, for mentioned scenarios, it is important to take the dynamic response of current loop into account. In line with this, the upcoming section will present the proposed sixth-order model, with the purpose of verifying theoretical findings and characterize transient stability.

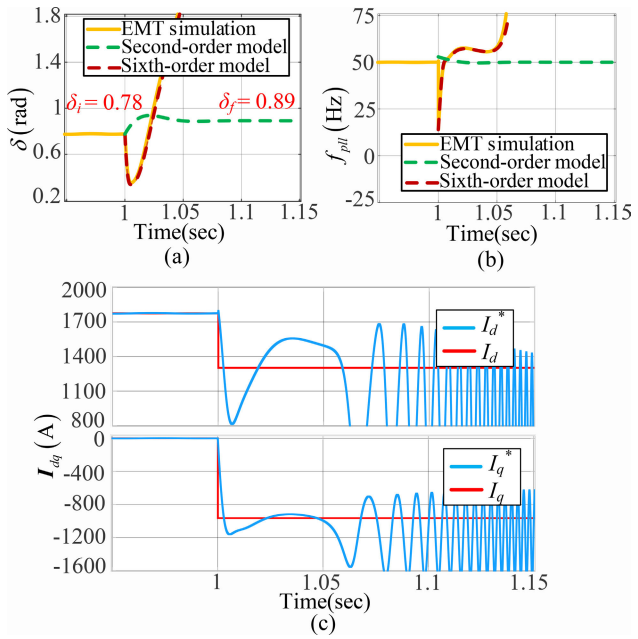

FIGURE 5. Dynamic response when u_{fault} is 0.66 p.u., L_g is 0.7 p.u., R_g is 0 p.u. and f_c = 150 Hz. (a) angle response, (b) frequency response and (c) current response.

III. SIXTH-ORDER TRANSIENT SYNCHRONIZATION MODEL

As seen in Figure 4(c) and 5(c), for the stated condition both active and reactive current exhibit slower response, thus phenomena is not captured by the second-order model. Therefore, to analyze the restrictions observed with the second-order model, (2) is reviewed to (7), thereby considered active

current variation (ΔI_d) as I_d-I_d^* and reactive current variation (ΔI_q) as I_q-I_q^*, and thus signify the impact of current dynamics.

$$\begin{cases} u_{pccd} = u_{gcp}\cos(\delta) - \omega_{pll} L_g \left(I_q^* + \Delta I_q\right) + L_g \Delta I_d' \\ u_{pccq} = -u_{gcp}\sin(\delta) + \omega_{pll} L_g \left(I_d^* + \Delta I_d\right) + L_g \Delta I_q' \end{cases} \tag{7}$$

Using (7), it is feasible to acquire the revised transient synchronization dynamics as follows

$$\delta = \int \left(K_{pp} + K_{ip}\int\right) \begin{pmatrix} -u_{gcp}\sin(\delta) + \omega_{pll} L_g \left(I_d^* + \Delta I_d\right) \\ +L_g \Delta I_q' \end{pmatrix} \tag{8}$$

$$\delta'' = \frac{K_{pp}\left(-u_{fault}\cos\delta\delta' + \left(\omega_g + \delta'\right) L_g \Delta I_d' + L_g \Delta I_q''\right)}{1 - K_{pp} L_g \left(I_d^* + \Delta I_d\right)} + \frac{K_{ip}\left(-u_{fault}\sin\delta + \left(\omega_g + \delta'\right)\left(I_d^* + \Delta I_d\right) L_g + L_g \Delta I_q'\right)}{1 - K_{pp} L_g \left(I_d^* + \Delta I_d\right)} \tag{9}$$

By examining (4) and (9), it observes that, there are additional variables in the angle dynamics. These variables are namely the incremental term ΔI_d and the differential term $L_g \Delta I_q{}'$, those additional variables in (9) amplify the level of interaction between the current control loop and the PLL, thereby influencing the transient stability prediction by the conventional second-order model.

Accordingly, integrating the plant equation (10) with the control equation (11), it is possible to derive the current dynamics as shown in (12).

$$\begin{cases} u_{pccd} = u_{gfcd} - \omega_{pll} L_f \left(I_q^* + \Delta I_q\right) + L_f \Delta I_d' \\ u_{pccq} = u_{gfcq} + \omega_{pll} L_f \left(I_d^* + \Delta I_d\right) + L_f \Delta I_q' \end{cases} \tag{10}$$

$$\begin{cases} u_{gfcd} = \left(K_{pc} + K_{ic}\int\right)\left[I_d^* - \left(I_d^* + \Delta I_d\right)\right] - \omega_g L_f \left(I_q^* + \Delta I_q\right) \\ u_{gfcq} = \left(K_{pc} + K_{ic}\int\right)\left[I_q^* - \left(I_q^* + \Delta I_q\right)\right] + \omega_g L_f \left(I_d^* + \Delta I_d\right) \end{cases} \tag{11}$$

$$\Delta I_d'' = \frac{-K_{pc}\Delta I_d' - K_{ic}\Delta I_d - \omega_g L_f \Delta I_q' + u_{fault}\sin\delta\delta'}{L_f + L_g} + \left(\omega_g + \delta'\right)\Delta I_q' + \left(I_q^* + \Delta I_q\right)\delta''$$

$$\Delta I_q'' = \frac{-K_{pc}\Delta I_q' + K_{ic}\left(I_q^* - \Delta I_q\right) + \omega_g L_f \Delta I_d' + u_{fault}\cos\delta\delta'}{L_f + L_g} - \left(\omega_g + \delta'\right)\Delta I_d' - \left(I_d^* + \Delta I_d\right)\delta'' \tag{12}$$

The sixth-order model (13), as shown at the bottom of the next page, is obtained by merging (9) and (12) to incorporate the current transient effect. This model is essential for illustrating the dynamic relationship between the current control loop and PLL. Moreover, the initial values of system can be calculated as (14), as shown at the bottom of the next page.

In (14), it is evident that the initial speed of the angle difference ($\delta_i{}'$) increases as a result of the strong connection between grid inductance and the initial speed of reactive current variation ($\Delta I_{qi}{}'$), that might harm transient stability [24]. Raising K_{pp} can increase the damping ratio of the system thereby improve transient stability [14], [21]. However, as seen in (14) simply increasing K_{pp} can actually amplify the $\Delta I_{qi}{}'$, leading to accelerate the $\delta_i{}'$, and thus posing a threat to transient stability. Accordingly, using the proposed sixth-order model, designers can determine the suitable f_c by setting current loop parameter while after setting the PLL parameters, and vice versa.

Transient stability analysis presented in this topic does not include any limiters; however, there exist study work which implemented frequency limiter in the output of PLL to restrict the error accumulated in the PI control, and to avoid an excessive frequency mismatch with the grid. Reference [27] found that, if an equilibrium point exists during the fault, frequency limiter degrades the synchronization stability by enlarging the transient peak phase; conversely if there is no equilibrium point existed, the frequency limiter lowers the transient peak phase and extends the critical clearing time.

During a severe fault, on the one hand, the converter transient frequency hits the limit, which constrains the speed of the phase change benefiting the stability; on the other hand, the restricted frequency also limits the error of the PLL controller and this will increase the settling time worsening the stability. Hereafter, [28] implement anti-windup strategy, in order to alleviate the negative effect of the frequency limiter on the synchronization stability, this also helps the PI controller would not accumulate the error after the saturation.

Since our paper mainly focuses on developing a model and examining the coupling mechanism of PLL and current control loop under weak grid scenario, the detailed analysis of frequency limiter and the implementation of anti-windup strategies is beyond the scope of this manuscript and it needs a further analysis. Therefore, upcoming research will establish the new model considering frequency limiter and anti-windup strategies to improve its overall effectiveness of study the area. Simulation and experimental work are presented in the subsequent sections to validate the accuracy of the proposed sixth-order model.

IV. ANALYSIS OF THE SIXTH ORDER MODEL

This section begins with the validation of the proposed mathematical model through simulations. It then proceeds to analyze the effect of controller parameters on both current control and PLL using sensitivity analysis.

A. VERIFICATION OF THE MATHEMATICAL MODEL

Ensuring the precision of the mathematical model outlined in equations (13) and (14) involves a comparison with a full order GFC model simulated in Matlab/Simulink. The mathematical model is solved using the 'ode45' solver in Matlab. The parameters for the GFC in Matlab/Simulink can be found in Table 1.

To verify the validity of the sixth-order model, the current dynamics under different current loop bandwidths during grid

TABLE 1. Circuit and controller parameters.

PARAMETER	Value	PARAMETER	Value
U_{nom}, Rated voltage	690 V	V_{dc}, DC-link voltage	1150 V
P_{nom}, Rated power	1.5 MW	L_f, Filter inductance	0.01 p.u.
K_{pp}, P gain of PLL	0.4	R_g, Grid resistance	0 p.u.
K_{ip}, I gain of PLL	25	L_g, Grid inductance	0.7 p.u.

faults are shown in Figure 6. The proposed model demonstrates precise capture of the current dynamics during grid faults.

Figure 7 illustrates the angle response with varying grid inductances. It is important to note that the accuracy of the sixth-order model remains unaffected by the change in L_g. Therefore, the sixth-order model is a reliable representation of the transient synchronization process.

B. PARAMETER SENSITIVITY ANALYSIS

The sensitivity analysis of the second and sixth order transient stability model is illustrated in Figure 8 and 9, respectively. This analysis examines the relation between the depth of voltage sag and grid stress in terms of short circuit ratio (SCR), and observes the impact of PLL and current controller parameter deviation on transient stability. The analysis is conducted using the parameter values provided in Table 1. The blue shaded area represents a stable zone, whereas the unshaded area indicates instability.

Figures 8(a) and 9(a) illustrate that both the second-order and sixth-order models indicate that LOS is more likely to happen at a low SCR value during a grid voltage drop fault.

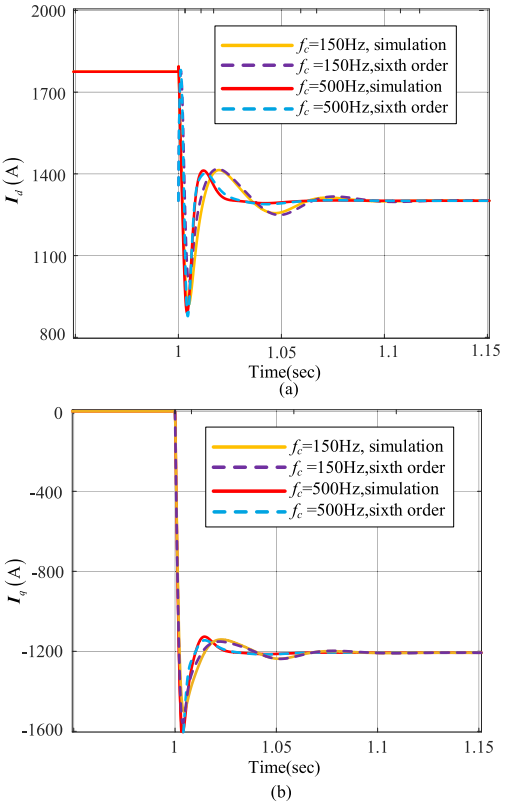

FIGURE 6. Current response under different current loop bandwidth, when u_{fault} of 0.66 p.u. and $L_g = 0.7$p.u.

Furthermore, the unstable region observed by the sixth-order model is larger than that of the second-order model. The

$$
\begin{cases}
\delta'' = K_{pp}\left(-u_{fault}\cos\delta\delta' + \left(\dfrac{L_g}{L_g+L_f}\right)\left(-K_{pc}\Delta I_q' + K_{ic}\left(I_q^* - \Delta I_q\right) + \omega_g L_f \Delta I_d' + u_{fault}\cos\delta\delta'\right)\right) + K_{ip}\left(-u_{fault}\sin\delta + \left(\omega_g + \delta'\right)\left(I_d^* + \Delta I_d\right)L_g + L_g\Delta I_q'\right) \\
\Delta I_q'' = \left(1 - \left(I_d^* + \Delta I_d\right)K_{pp}L_g\right)\left(\dfrac{-K_{pc}\Delta I_q' + K_{ic}\left(I_q^* - \Delta I_q\right) + \omega_g L_f \Delta I_d' + u_{fault}\cos\delta\delta'}{L_g + L_f}\right) - \left(\omega_g + \delta'\right)\Delta I_d' - \left(I_d^* + \Delta I_d\right)\left(\begin{array}{l} K_{pp}\left(-u_{fault}\cos\delta\delta'\right) \\ +K_{ip}\left(-u_{gcp}\sin\delta + \left(\omega_g + \delta'\right)\left(I_d^* + \Delta I_d\right)L_g + L_g\Delta I_q'\right)\end{array}\right) \\
\Delta I_d'' = \dfrac{-K_{pc}\Delta I_d + K_{ic}\left(I_d^* - \Delta I_d\right) - \omega_g L_f \Delta I_q' + u_{fault}\sin\delta\delta'}{L_g + L_f} + \left(\omega_g + \delta'\right)\Delta I_q' + \left(I_q^* + \Delta I_q\right)\left(\begin{array}{l} K_{pp}\left(-u_{fault}\cos\delta\delta' + \left(\dfrac{L_g}{L_g+L_f}\right)\left(\begin{array}{l} -K_{pc}\Delta I_q' + K_{ic}\left(I_q^* - \Delta I_q\right) \\ +\omega_g L_f \Delta I_d' + u_{fault}\cos\delta\delta'\end{array}\right)\right) \\ +K_{ip}\left(-u_{fault}\sin\delta + \left(\omega_g + \delta'\right)\left(I_d^* + \Delta I_d\right)L_g + L_g\Delta I_q'\right)\end{array}\right)
\end{cases}
\tag{13}
$$

$$
\begin{cases}
\delta_i = \sin^{-1}\dfrac{\omega_{pll}L_g I_d}{u_{gcp}} \\
\Delta I_{di} = 0 \\
\Delta I_{qi} = 0 \\
\delta_i' = \dfrac{K_{pp}\left(-u_{fault}\sin\delta_i + \omega_g L_g I_d^* + L_g\Delta I_{qi}'\right)}{1 - K_{pp}L_g I_d^*} \\
\Delta I_{di}' = \dfrac{K_{pc}I_d^* - \omega_g L_f I_q^* - u_{fault}\cos\delta_i}{L_g + L_f} + \left(\omega_g + \delta_i'\right)I_q^* \\
\Delta I_{qi}' = \dfrac{K_{pc}\left(I_q^*\right) + \omega_g L_f I_d^* + u_{fault}\sin(\delta_i)}{L_f + L_g} - \left(\omega_g + \delta_i'\right)I_d^*
\end{cases}
\tag{14}
$$

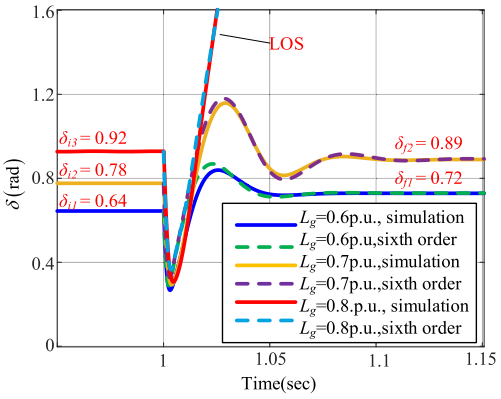

FIGURE 7. Angle response with different L_g when f_c is 150Hz.

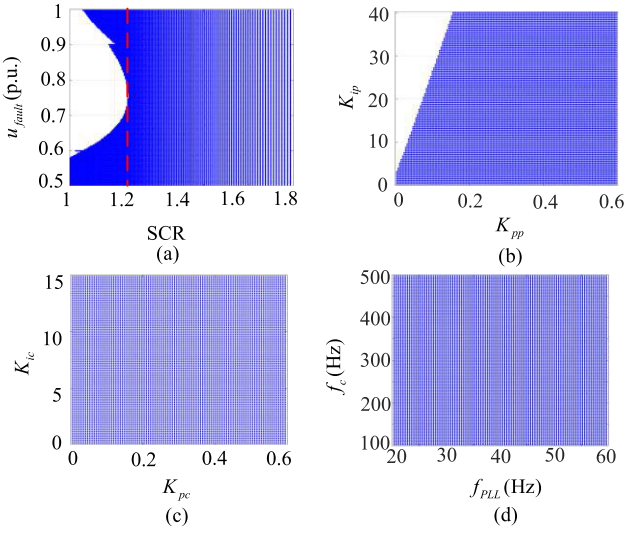

FIGURE 8. Second-order model parameter sensitivity results.

second-order model's estimation might be inaccurate or misjudged when encountering a slight voltage drop at a lower SCR value. Consequently, weak grid connected GFC with a lower f_c setting may experience LOS due to a minor grid voltage drop.

According to Figure 8(b), decreases the K_{pp} while increases the K_{ip} results in LOS, since the damping ratio of the PLL is reduced. Conversely, increases both K_{pp} and K_{ip} enables to improve stability region.

Nevertheless, it is important to note that this inference may not hold true in some extent, when weak grid connected GFC while operating under a lower f_c. Figure 9(b) illustrates that, the sixth-order model tends to experience LOS, when both the K_{pp} and K_{ip} are increased simultaneously. Figure 8(c), the change of current loop parameters has a negligible impact on the transient synchronization stability of the second-order model. Conversely, Figure 9(c) reveals that a simultaneous reduction or increase in the proportional parameters of the current control loop is more likely to result in a LOS.

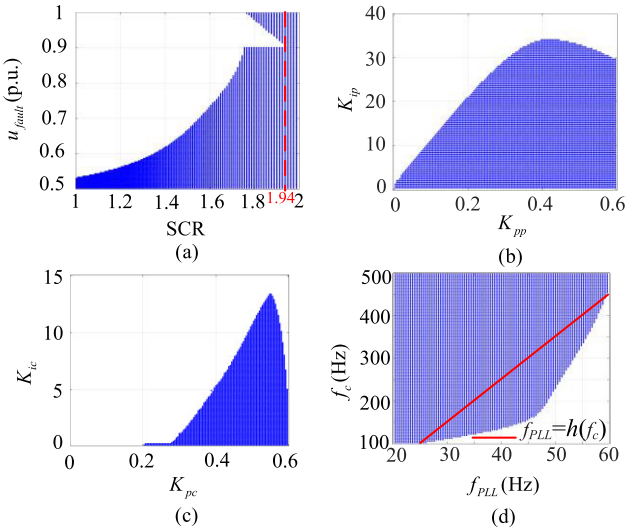

FIGURE 9. Sixth-order model parameter sensitivity results.

The bandwidth pair (f_{PLL}, f_c) that can maintain the synchronization stability during the transient process of the system, namely the attraction region as showed by the blue area in Figure.8(d) and Figure 9(d). Accordingly, if we are using the second-order model to determine the attraction region, consequently the output frequency's convergence across various PLL bandwidths is independent of the current loop bandwidth and is only influenced by the parameters of the PLL itself. Therefore, the resulting attraction region is rectangular, with its sides aligned parallel to the horizontal axis as shown by Figure 8(d), indicating no correlation with the current loop bandwidth. However, while using sixth-order model, since the convergence of the system in this situation is related to the value of the current loop bandwidth, the boundary is a curving segment.

$$f_c > 10 f_{PLL} - 150 = h(f_c) \tag{15}$$

As seen in Figure 9(d), when the current loop bandwidth is much larger than the PLL bandwidth, a conservative curve fitting is carried out, and it has been observed that when the ratio of the current loop bandwidth to PLL bandwidth aligns with the fitting curve denoted as $h(f_c)$ in (15), the dynamics of the current can be ignored in the analysis of transient stability.

In general, the attraction region shown in Figure 9(d) obtained through sixth-order model is smaller than that of the second-order model as shown by Figure 8(d), this indicates that, the current dynamics in the weak inductive grid will reduce the transient stability.

Furthermore, in this paper, we analyze the critical bandwidth and voltage dip that cause a loss of synchronization, can be calculated using the sixth-order model, and the results are presented in Figure 10. Accordingly, when the grid voltage drops to 0.6 p.u. while f_c = 150Hz, as shown by point-**a**, it lays in the blue region, this shows, result is consistent with those obtained through EMT simulation and the sixth-order model, as discussed previously. Conversely, when the grid

voltage drops to 0.65p.u. while $f_c = 150$Hz, as shown by the point-**b**, it lays out of blue region, which indicate that the system is unstable, this result is also consistent too with the result that obtain through EMT simulation and sixth-order model.

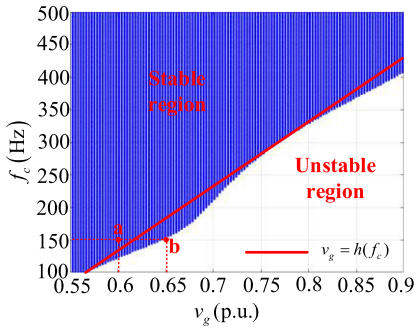

FIGURE 10. Current loop bandwidth versus voltage sag when the damping ratio (ζ) = 0.707.

Furthermore, Figure 10 illustrates that as the voltage dip becomes more severe, the stability region that maintains transient stability expands. This is due to the increase in injection of reactive current by the GFC into the system, as stated by the grid code, this elevates the PCC voltage level, thereby ensuring the system remains stable.

$$f_c > 984.8V_g - 461.36 = h(f_c) \tag{16}$$

In general, as seen by Figure 10, there is no consistent ratio between the current loop bandwidth and the voltage dip, to obtain critical current loop bandwidth for the specific voltage dip, conservative curve fitting is carried out, and it has been observed that when the ratio aligns with the fitting curve denoted as $h(f_c)$ in (16), the dynamics of the current can be ignored in the analysis of transient stability.

In the following parts, the proposed sixth-order model will be verified by the experimental results. Thus, the sixth-order transient synchronization model considering the current loop proposed in this article is of great significance in guiding the design of current controller parameters. For example, after setting the bandwidth of PLL, designers can solve out the suitable bandwidths of the current loop using this sixth-order model, and vice versa.

V. EXPERIMENTAL VERIFICATION

The control-hardware-in-loop platform is utilized to acquire the experimental results, Figure 11 is shown the experimental setup, where 1.5-MW GFC model is developed in Typhoon 602+ with a time step of 1 μs. TMS320F28335/Spartan6 XC6SLX16 DSP + FPGA control board is used to implement the control strategies. The circuit and controller parameters are established in accordance with the information presented in Table 1.

To verify the impact of current loop on transient stability while under different f_c, the parameters are set to $u_{fault} =$ 0.66 p.u., the injected current is based on grid code, PLL

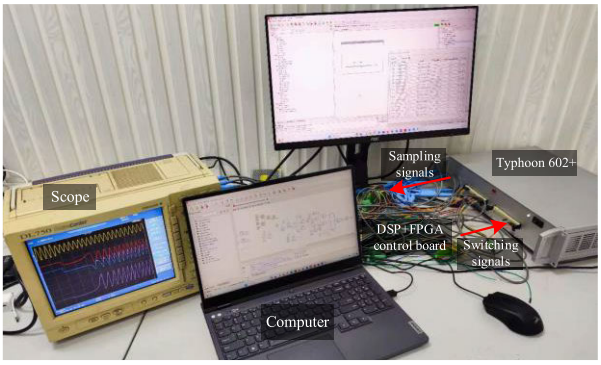

FIGURE 11. Configuration of the experimental setup.

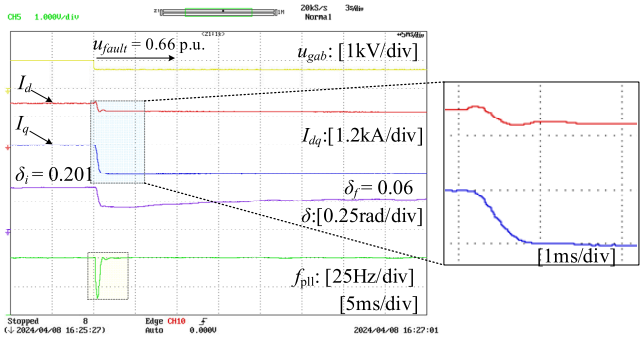

(a)

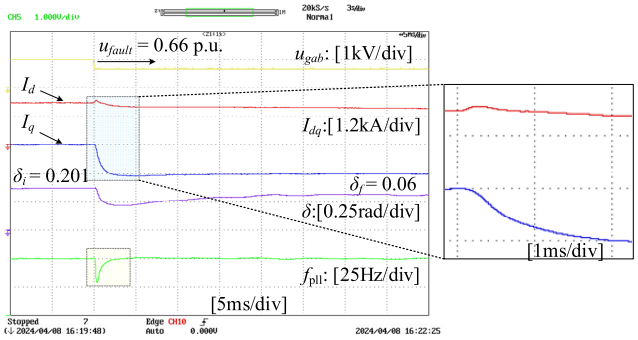

(b)

FIGURE 12. Experimental results to study the impact of current controller when $u_{fault} = 0.66$ p.u., $L_g = 0.2$ p.u. and $R_g = 0.2$ p.u., (a) $f_c = 500$Hz, (b) $f_c = 150$Hz.

bandwidth (f_{pll}) is configured at 50 Hz, and 150 Hz and 500 Hz are used for slower and faster f_c, respectively.

Figure 12, illustrates experimental results of stiff grid configuration, with parameters of $L_g = 0.2$ p.u. and $R_g = 0.2$ p.u., accordingly when $f_c = 500$Hz, as seen in Figure 12(a), the injected current completes the transient process within less than 1ms. Likewise, when $f_c = 150$ Hz, as seen in Figure 12(b) the injected current completes the transient process within less than 2 ms. Therefore, in the case of a stiff grid condition, no matter how f_c is faster or slower the system

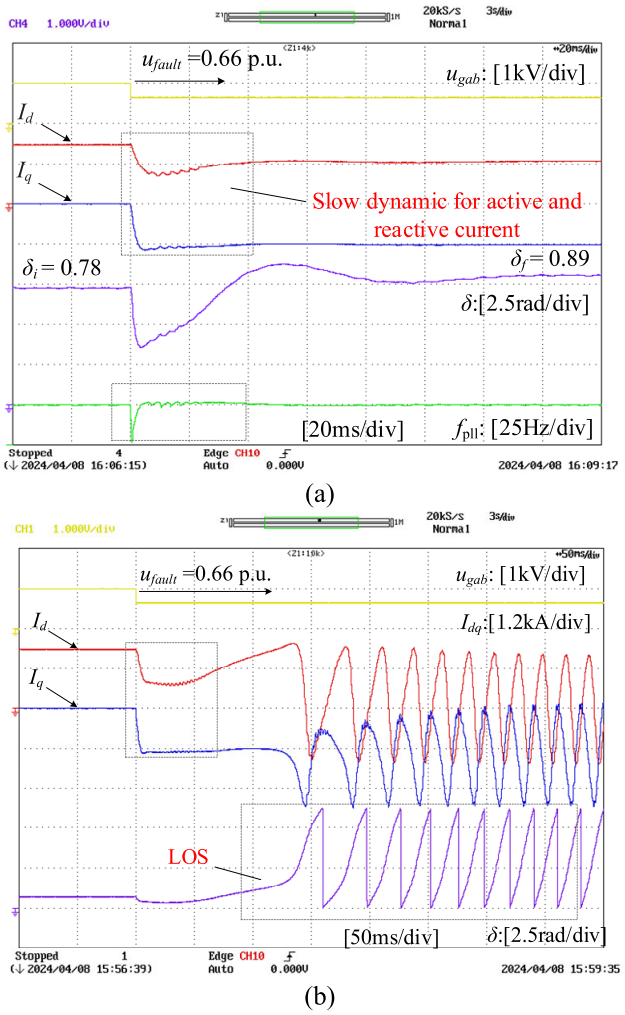

FIGURE 13. Experimental results to study the impact of current controller when u_{fault} = 0.66 p.u., L_g = 0.7 p.u. and R_g = 0 p.u., (a) f_c = 500Hz, (b) f_c = 150Hz.

is always stable, i.e, f_c has insignificance effect on transient stability.

Figure 13, illustrates experimental result of weak grid condition with parameters of $L_g = 0.7$ p.u., $R_g = 0$ p.u., accordingly when f_c is 500 Hz, as seen in Figure 14(a), the injected current dynamics is exhibited slow transient response which lasts around 40ms, also seen a notable fluctuation in angle difference. Likewise, when $f_c = 150$ Hz, the current transient response is become more slower, and is lasted more than 50ms resulting in LOS in GFC, observed in Figure 13(b). Accordingly, the experimental results are consistent with simulation results.

VI. CONCLUSION

When weak grid with slower current loop bandwidth setting exposed to a narrow grid voltage drop fault, PLL would dynamically couple with both active and reactive current transient during the synchronization process. This paper developed a sixth-order transient model to accurately judge the stable range with parameter deviation. Based on the proposed model, this paper observes that a lower current loop bandwidth further accelerates the movement of the phase angle difference under weak grid conditions, leading to loss of synchronization (LOS) and PLL frequency divergence. Additionally, the proposed sixth-order model offers the advantage of conveniently adjusting the current loop parameter after configuring the PLL parameters.

REFERENCES

[1] H. Li, H. Nian, B. Hu, Y. Wang, and M. Li, "A noise interference suppression method with optimized frequency adjustment for impedance measurement," *IEEE Trans. Ind. Electron.*, vol. 71, no. 12, pp. 15924–15933, Dec. 2024, doi: 10.1109/tie.2024.3395760.

[2] Z. Xu, Y. Qi, J. M. Guerrero, J. C. Vasquez, Y. Wang, H. Zhao, W. Li, and Y. Wu, "Stability-oriented impedance modeling, analysis, and shaping for power supply system in more-electric aircraft: A review," *IEEE Trans. Transport. Electrific.*, early access, Aug. 8, 2024, doi: 10.1109/TTE.2024.3369329.

[3] L. Zhan, B. Hu, L. Chen, Y. Liao, M. Li, and H. Nian, "Transient stability enhancement of current limited-GFM inverters based on varying virtual impedance," *IEEE Trans. Ind. Electron.*, vol. 71, no. 12, pp. 15946–15958, Dec. 2024.

[4] M. G. Taul, X. Wang, P. Davari, and F. Blaabjerg, "Reduced-order and aggregated modeling of large-signal synchronization stability for multi-converter systems," *IEEE J. Emerg. Sel. Topics Power Electron.*, vol. 9, no. 3, pp. 3150–3165, Jun. 2021.

[5] J. Hu, Q. Hu, B. Wang, H. Tang, and Y. Chi, "Small signal instability of PLL-synchronized type-4 wind turbines connected to high-impedance AC grid during LVRT," *IEEE Trans. Energy Convers.*, vol. 31, no. 4, pp. 1676–1687, Dec. 2016.

[6] F. Blaabjerg, Y. Yang, D. Yang, and X. Wang, "Distributed power-generation systems and protection," *Proc. IEEE*, vol. 105, no. 7, pp. 1311–1331, Jul. 2017.

[7] E. O. N. Netz, *Grid Code-High and Extra High Voltage*. Bayreuth, Germany: E. Netz GmbH, Apr. 2006.

[8] *Technical Rule for Connecting Wind Farm to Power System*, Standard Chinese Standard GB/T 19963-2011, 2011.

[9] Y. Ma, D. Zhu, Z. Zhang, X. Zou, J. Hu, and Y. Kang, "Modeling and transient stability analysis for type-3 wind turbines using singular perturbation and Lyapunov methods," *IEEE Trans. Ind. Electron.*, vol. 70, no. 8, pp. 8075–8086, Aug. 2023.

[10] P. Hu, Z. Chen, Y. Yu, and D. Jiang, "On transient instability mechanism of PLL-based VSC connected to a weak grid," *IEEE Trans. Ind. Electron.*, vol. 70, no. 4, pp. 3836–3846, Apr. 2023.

[11] Q. Hu, L. Fu, F. Ma, and F. Ji, "Large signal synchronizing instability of PLL-based VSC connected to weak AC grid," *IEEE Trans. Power Syst.*, vol. 34, no. 4, pp. 3220–3229, Jul. 2019.

[12] M. G. Taul, X. Wang, P. Davari, and F. Blaabjerg, "Systematic approach for transient stability evaluation of grid-tied converters during power system faults," in *Proc. IEEE Energy Convers. Congr. Expo. (ECCE)*, Sep. 2019, pp. 5191–5198.

[13] D. Dong, B. Wen, D. Boroyevich, P. Mattavelli, and Y. Xue, "Analysis of phase-locked loop low-frequency stability in three-phase grid-connected power converters considering impedance interactions," *IEEE Trans. Ind. Electron.*, vol. 62, no. 1, pp. 310–321, Jan. 2015.

[14] H. Wu and X. Wang, "Design-oriented transient stability analysis of PLL-synchronized voltage-source converters," *IEEE Trans. Power Electron.*, vol. 35, no. 4, pp. 3573–3589, Apr. 2020.

[15] M. G. Taul, X. Wang, P. Davari, and F. Blaabjerg, "An efficient reduced-order model for studying synchronization stability of grid-following converters during grid faults," in *Proc. 20th Workshop Control Modeling Power Electron. (COMPEL)*, Toronto, ON, Canada, Jun. 2019, pp. 1–7.

[16] H. Wu and X. Wang, "Transient stability impact of the phase-locked loop on grid-connected voltage source converters," in *Proc. Int. Power Electron. Conf. (IPEC-Niigata -ECCE Asia)*, May 2018, pp. 2673–2680.

[17] Ö. Göksu, R. Teodorescu, C. L. Bak, F. Iov, and P. C. Kjær, "Instability of wind turbine converters during current injection to low voltage grid faults and PLL frequency based stability solution," *IEEE Trans. Power Syst.*, vol. 29, no. 4, pp. 1683–1691, Jul. 2014.

[18] S. Ma, H. Geng, G. Yang, and B. Liu, "Experimental validation of adaptive current injecting method for grid-synchronization improvement of grid-tied REGS during short-circuit fault," in *Proc. Int. Power Electron. Conf. (IPEC-Niigata-ECCE Asia)*, May 2018, pp. 542–546.
[19] C. Wu, X. Xiong, M. G. Taul, and F. Blaabjerg, "Enhancing transient stability of PLL-synchronized converters by introducing voltage normalization control," *IEEE J. Emerg. Sel. Topics Circuits Syst.*, vol. 11, no. 1, pp. 69–78, Mar. 2021.
[20] J. Pei, J. Yao, Y. Liu, S. Chen, P. Sun, and S. Huang, "Modeling and transient synchronization stability analysis for PLL-based renewable energy generator considering sequential switching schemes," *IEEE Trans. Power Electron.*, vol. 37, no. 2, pp. 2165–2179, Feb. 2022.
[21] B. Hu, C. Zhao, S. Sahoo, C. Wu, L. Chen, H. Nian, and F. Blaabjerg, "Synchronization stability enhancement of grid-following converter under inductive power grid," *IEEE Trans. Energy Convers.*, vol. 38, no. 2, pp. 1485–1488, Jun. 2023.
[22] J. Chen, M. Liu, T. O'Donnell, and F. Milano, "Impact of current transients on the synchronization stability assessment of grid-feeding converters," *IEEE Trans. Power Syst.*, vol. 35, no. 5, pp. 4131–4134, Sep. 2020.
[23] C. Wu, Y. Lyu, Y. Wang, and F. Blaabjerg, "Transient synchronization stability analysis of grid-following converter considering the coupling effect of current loop and phase locked loop," *IEEE Trans. Energy Convers.*, vol. 39, no. 1, pp. 544–554, Mar. 2024.
[24] B. Hu, L. Zhan, S. Sahoo, L. Chen, H. Nian, and F. Blaabjerg, "Synchronization stability analysis under ultra-weak grid considering reactive current dynamics," *IEEE Trans. Ind. Electron.*, vol. 71, no. 11, pp. 15220–15223, Nov. 2024.
[25] J. Jankovskis, D. Stepins, and D. Pikulins, "Effects of increasing switching frequency in frequency modulated power converters," in *Proc. 9th Int. Symp. Electron. Telecommun.*, Timisoara, Romania, Nov. 2010, pp. 115–118.
[26] C.-H. Tsai, B.-M. Chen, and H.-L. Li, "Switching frequency stabilization techniques for adaptive on-time controlled buck converter with adaptive voltage positioning mechanism," *IEEE Trans. Power Electron.*, vol. 31, no. 1, pp. 443–451, Jan. 2016.
[27] J. Chen, M. Liu, H. Geng, T. O'Donnell, and F. Milano, "Impact of PLL frequency limiter on synchronization stability of grid feeding converter," *IEEE Trans. Power Syst.*, vol. 37, no. 3, pp. 2487–2490, May 2022.
[28] M. A. A. Murad and F. Milano, "Modeling and simulation of PI-controllers limiters for the dynamic analysis of VSC-based devices," *IEEE Trans. Power Syst.*, vol. 34, no. 5, pp. 3921–3930, Sep. 2019.

TEKLU DEREJE was born in Dire Dawa, Ethiopia. He received the B.Sc. degree in electrical electronics technology and the M.Sc. degree in industrial automation and control technology from Adama Science and Technology University, Adama, Ethiopia, in 2009 and 2015, respectively. He is currently pursuing the Ph.D. degree in electrical engineering with Zhejiang University. His research interest includes transient stability analysis on power electronics converters.

LING ZHAN was born in Wenzhou, China. He received the B.Eng. degree in electrical engineering from Zhejiang University, Hangzhou, China, in 2022, where he is currently pursuing the Ph.D. degree in electrical engineering. His research interest includes transient stability analysis on power converters.

BIN HU (Member, IEEE) was born in Wenzhou, China. He received the B.Eng. degree in electrical engineering from Shenyang University of Technology, Shenyang, China, in 2018, and the Ph.D. degree in electrical engineering from Zhejiang University, Hangzhou, China, in 2023. His research interest includes large-signal and small-signal stability analysis of converter-based resources, especially doubly fed induction generator-based wind power systems.

HENG NIAN (Senior Member, IEEE) received the B.Eng. and M.Eng. degrees in electrical engineering from Hefei University of Technology, Hefei, China, in 1999 and 2002, respectively, and the Ph.D. degree in electrical engineering from Zhejiang University, Hangzhou, China, in 2005. Since 2016, he has been a Full Professor with the College of Electrical Engineering, Zhejiang University. His current research interests include the optimal design and operation control for wind power generation systems.